Heavy-ion charge exchange reaction $^{28}Si(^{18}O,^{18}F)^{28}Al$

B. T. Kim, A. Greiner, M. A. G. Fernandes,* N. Lisbona, K. S. Low,† and M. C. Mermaz
DPh-N/BE, CEN Saclay, BP 2, 91190 Gif-sur-Yvette, France
(Received 25 April 1979)

The angular distribution has been measured for the 3^+ and 2^+ ground state doublet in ^{28}Al with the heavy-ion charge exchange reaction $^{28}Si(^{18}O,^{18}F)^{28}Al$ at the incident beam energy of 56 MeV. It has been analyzed in terms of the microscopic one-step direct charge exchange model and the second-order DWBA approach with recoil effect taking into account the two-step successive transfer: one nucleon stripping and pickup, and pickup and stripping process. The general shape of angular distribution has been reproduced by both approaches. The strength of the spin-isospin dependent two-body interaction potential extracted from one-step calculations is close to the upper limit of uncertainties reported in the light-ion charge exchange experiment. The two-step mechanism turns out to be also important and could be a competing process.

[NUCLEAR REACTION $^{28}Si(^{18}O, ^{18}F)$, $E=56$ MeV; measured $\sigma(\theta)$; microscopic DWBA analysis; second-order DWBA analysis with recoil effect; deduced strength of the $(\vec{\sigma}\cdot\vec{\sigma})(\vec{\tau}\cdot\vec{\tau})$ term in the nucleon-nucleon two-body force.]

I. INTRODUCTION

The charge exchange mode in light-ion reactions has become[1,2] evident and has appeared as a useful tool for studying the intrinsic isospin collective motion. However, several light-ion experiments have shown[3-7] that the direct one-step charge exchange due to the Majorana term in the two-body interaction is not necessarily the dominant reaction process and thus the multi-step mechanisms, such as core excitation[5] and successive transfer[6,7] rather than the usual one-step mechanism, are adequate for explaining the experimental results. The validity of the quantitative spectroscopic values obtained from the direct charge exchange thus becomes dubious. Another problem which reduces potentiality of the charge exchange experiment as a spectroscopic tool is the lack of information about the Majorana term in the nucleon-nucleon force.

It is still an interesting topic whether the charge exchange in the nuclear reaction occurs via a direct charge exchange mode or is dominated by the multi-step successive transfer. The use of heavy ions to investigate this topic has some advantages: (1) The heavy ion induced charge exchange usually includes a spin as well as an isospin transfer and thus is more selective than the light-ion reaction. For example, the $(^{18}O,^{18}F)$ reaction gives both spin and isospin transfer of 1 and thus only the $(\vec{\sigma}\cdot\vec{\sigma})(\vec{\tau}\cdot\vec{\tau})$ term in the two-body force contributes to the direct charge exchange process. Furthermore, (2) there are usually more open channels in a heavy-ion reaction than in a light reaction, and this increases the probability of multi-step processes. Few heavy-ion charge exchange experiments, however, have been done so far, because the experimental cross sections are generally small and partly because the analysis of data is too much involved, especially for the multi-step processes. Nonetheless, the very light heavy-ion induced reactions, such as the $(^6Li,^6He)$[8,9] and $(^7Li,^7Be)$ reaction,[10] have been performed and they showed that the direct charge exchange mode is favorable over the multi-step processes, but some possibilities of multi-step processes are not excluded for large angular momentum transfer even though the multi-step calculations are not presented explicitly.

In this paper we present a study of the charge exchange reaction $^{28}Si(^{18}O,^{18}F)^{28}Al$ at 56 MeV. This reaction can be easily understood in terms of a one-step direct charge exchange mechanism. With a very simple shell model in mind, it can be interpreted that a neutron of the ^{18}O in the $J^\pi=0^+$, $T=1$ state interacts with a proton in the $d_{5/2}$ shell of ^{28}Si and they exchange their spin and charge forming $J^\pi=1^+$, $T=0$ ^{18}F, and $J^\pi=3^+$ or 2^+, $T=1$ ^{28}Al. In addition this particular choice of the $^{18}O + ^{28}Si$ system gives many open reaction channels and helps in the study of the contributions from multi-step processes. In fact we have also studied other transfer channels (see Appendix), and have integrated them into our second order distorted-wave Born-approximation (DWBA) calculations.

In the present analysis of data, we have first performed the direct charge exchange DWBA calculations. These results are compared with the exact-finite-range (EFR) second order DWBA calculations which take into account the successive one-nucleon stripping and pickup, and pickup and stripping process. A brief summary of the direct charge exchange DWBA formalism and second order EFR-DWBA approach is given in Sec. III. We

 © 1979 The American Physical Society

present our results of numerical analysis in Sec. IV. Finally, general conclusions are summarized in Sec. V.

II. EXPERIMENTAL PROCEDURE

The experiments have been performed using a 56 MeV ^{18}O ion beam of the FN tandem Van de Graaff of Saclay. The angular distributions have been measured using a quadrupole dipole dipole dipole (QDDD) magnetic spectrometer. A two-stage gas proportional counter was used in order to measure the position and to identify the heavy fragments. The total length of the counter was 50 cm. The 99% enriched ^{28}Si target on a carbon backing had a thickness of 165 μg/cm^2. The kinematic corrections made by a quadrupole system allowed us to reach a resolution of 140 keV full width at half maximum (FWHM). The horizontal aperture of the spectrometer in the reaction plane was 3° and the vertical aperture was 7°.

Only the 3^+ and 2^+ ground state doublet in ^{28}Al has been studied. The higher states were not resolved in this experiment. The angular distribution of the ground state doublet in ^{28}Al has been measured between 5° (lab angle) and 29° in 2° steps.

The cross sections were corrected using a formula given by Marion and Young[11] for the charge state distribution. It has been verified[12] that these values agree well with experimental ones. The absolute values of the cross sections are obtained by normalizing the charge exchange reaction data to the elastic scattering at far forward angles where deviations from Rutherford scattering are negligible.

III. CHARGE EXCHANGE THEORY

A. Higher order Born approximation

In the present section we briefly summarize formulas needed for calculating differential cross sections for successive as well as one-step transfer reactions in terms of the higher order Born approximation. Since such a formulation has been shown in detail by a number of authors,[7,13,14] we only present here the necessary relations for numerical calculations very closely following Ref. 14.

The reaction processes we have in mind may be symbolized by $a+A \to b+B \to c+C \cdots$ where each step can be any one-step direct reaction including direct charge exchange. We denote the channel indices α, β, γ, etc., for the partitions $a+A$, $b+B$, $c+C$, etc. We further use the so-called $(J_\gamma l_c, l_a)$ representation, where J_γ stands for a set of transferred angular momenta $(j_\gamma, l_\gamma, s_\gamma)$ in a transition $a+A \to c+C$, and l_c's are the possible partial waves in the channel γ for a given partial wave l_a in the incident channel.

From the coupled reaction channel (CRC) equations for the partial distorted wave $\chi_{J_\beta l_b, l_a}$, one can obtain[14] a set of inhomogeneous equations for the ith order distorted waves $\chi^{(i)}_{J_\beta l_b, l_a}$ with the source term generated by the $(i-1)$th order waves $\chi^{(i-1)}_{J_\gamma l_c, l_a}$ as

$$D_\beta(r_b)\chi^{(i)}_{J_\beta l_b, l_a}(r_b) = \sum_{J_\gamma l_c} \mathcal{J} \int dr_c r_c r_b F_{J_\beta l_b, J_\gamma l_c, l_a} \times (r_b, r_c)\chi^{(i-1)}_{J_\gamma l_c, l_a}(r_c), \tag{1}$$

where

$$D_\beta = \frac{\hbar^2}{2\mu_\beta}\left[\frac{d^2}{dr_b^{\,2}} - \frac{l_b(l_b+1)}{r_b^{\,2}}\right] - U_\beta + E_\beta \tag{2}$$

and $\mathcal{J}$ is the Jacobian. F are just products of the form factor $F^{jls}_{l_b, l_c}(r_b, r_c)$ and geometrical factors as defined in Eq. (2.14) of Ref. 14. The exact finite range form factor $F^{jls}_{l_b, l_c}$ can be evaluated according to Ref. 15. Nevertheless we will present the microscopic charge exchange form factor in the next subsection. The U_β in Eq. (2) is the distorting one-body optical potential, and $E_\beta = E - \epsilon_\beta$, where E and ϵ_β denote the total energy of the system and the intrinsic energy in the channel β, respectively.

Equation (1) can be solved in an iterative way starting with the zeroth order which is nothing but the usual optical model distorted wave in the incident channel with the boundary condition that there is an incoming wave as well as outgoing waves. The higher order solution can thus be obtained with the usual outgoing boundary condition

$$\chi^{(i)}_{J_\beta l_b, l_c}(r_b) \to \hat{l}_b e^{-i\sigma_{l_b}} \left(\frac{v_\alpha}{v_\beta}\right)^{1/2} \frac{k_\alpha}{k_\beta} \times C^{(i)}_{J_\beta l_b, l_a}[G_{l_b}(r_b) + iF_{l_b}(r_b)], \tag{3}$$

where F_l and G_l are the regular and irregular Coulomb functions, k is the channel wave number, and σ_l the Coulomb phase shift. With this C matrix, the transition amplitude can be given as

$$T_{m_b M_B, m_a M_A} = \sum_{jls}\sum_{l_a l_b} \frac{1}{k_\beta} (l_a 0 l_b m_{l_b} | lm_l) \hat{l}_b e^{2i\sigma_{l_b}} h(\beta\alpha; jls) \times \sum_i C^{(i)}_{J_\beta l_b, l_a} Y_{l_b m_{l_b}}(\theta_{l_b}, 0) \tag{4}$$

and

$$h(\beta\alpha, jls) = (-)^{I_A - M_A + s_b - m_b + s + m_s} (I_A M_A I_B - M_B | jm_j) \times (s_a m_a s_b - m_b | sm_s)(jm_j sm_s | l - m_l). \tag{5}$$

The first-order solution gives a transition ampli-

tude equivalent to that of usual DWBA for a direct one-step reaction $a+A\to b+B$. For a two-step process $a+A\to c+C\to b+B$, the second order solution gives a transition amplitude corresponding to the second order DWBA, and so on. The cross section can finally be written as

$$\frac{d\sigma}{d\Omega}=\frac{1}{(2I_A+1)(2s_a+1)}\sum_{m_bM_B,\,m_aM_A}|T_{m_bM_B,\,m_aM_A}|^2 . \quad (6)$$

B. Microscopic form factor for the direct charge exchange

We review the microscopic theory for the direct charge exchange process induced by heavy-ions very briefly. Since charge exchange is considered as inelastic scattering, which does not cause a change of mass number but changes both spin and isospin in the target and projectile nucleus, this treatment does not raise the finite-range problem. We also neglect the "knock-on" process of which contributions seem to be small[1] because of a poor spatial overlap of the wave functions in the target and projectile system. The EFR form factor then becomes simply the inelastic form factor[9,16] which takes into account both spin and isospin transitions.

The most general form of the form factor may be given as

$$F(\vec{R})=\langle I_BM_BT_BN_B;s_bm_bt_bn_b|\,V\,|t_an_as_am_a;T_AN_AI_AM_A\rangle , \quad (7)$$

where the additional quantum numbers $T(N)$ and $t(n)$ are attached to designate the isospin (its projection) of the target and projectile, respectively. The bracket in Eq. (7) is understood to integrate over all the internal coordinates of the target and projectile. The interaction potential V, which is assumed as the central force in the present approach, thus produces the spin and isospin excitation. In a microscopic description, we may write it in terms of the net effective two-body nucleon-nucleon interaction between nucleons in the projectile and target as

$$V=\sum_{\substack{i\in A\\ j\in a}} v_{ij}(|\vec{r}_j-\vec{r}_i+\vec{R}|) \quad (8)$$

and

$$v_{ij}=v(|\vec{r}_j-\vec{r}_i+\vec{R}|)\sum_{\substack{s_0m_0\\ t_0n_0}} V_{s_0t_0}(-)^{m_0+n_0}\times\sigma^{s_0}_{-m_0}(i)\sigma^{s_0}_{m_0}(j)\tau^{t_0}_{-n_0}(i)\tau^{t_0}_{n_0}(j) , \quad (9)$$

where σ and τ are the unit operators when $s_0=t_0=0$, whereas they become the spin and isospin Pauli operators, respectively, when $s_0=t_0=1$. $V_{s_0t_0}$ denotes the strength of the interaction potential. By performing a multipole decomposition the form factor $F(\vec{R})$ becomes in the usual manner[15]

$$F(\vec{R})=\sum_{\substack{jls\\ m_jm_lm_s}} i^{-l}\hat{s}_a\hat{I}_Bh(\beta\alpha;jls)\sqrt{4\pi}\,F^{jls}_{m_l}(\vec{R}) . \quad (10)$$

We have singled out $\sqrt{4\pi}$ so as to have the same radial form factor as appeared in Ref. 15. Now $F^{jls}_{m_l}(\vec{R})$ in the coordinates shown in Fig. 1 is

$$F^{jls}_{m_l}(\vec{R})=\sum_{l_1l_2s_0t_0n_0} V_{s_0t_0}d^{jls;\,l_1l_2s_0t_0n_0}f^{jls;\,l_1l_2s_0t_0}_{m_l}(\vec{R}) , \quad (11)$$

where

$$d^{jls;\,l_1l_2s_0t_0n_0}=i^{l_2+l-l_1}(-)^{s_a-s_b}\hat{s}_a^{-1}\hat{s}_bW(l_1l_2js;ls_0)\times(-)^{n_0}(T_AN_At_0n_0|\,T_BN_B)(t_an_at_0-n_0|\,t_bn_b) \quad (12)$$

and

$$f^{jls;\,l_1l_2s_0t_0}_{m_l}(\vec{R})=\frac{1}{\sqrt{4\pi}}\int\int d\vec{r}_1d\vec{r}_2v(|\vec{r}_2-\vec{r}_1+\vec{R}|)\times g^{l_1s_0j,\,t_0}_{AB}(r_1)g^{l_2s_0s,\,t_0}_{ab}(r_2)\times[Y^*_{l_1}(\hat{r}_1)Y_{l_2}(\hat{r}_2)]_{lm_l} , \quad (13)$$

where $\vec{r}_1$ and $\vec{r}_2$ are the coordinates for the interacting nucleons in the target and projectile, respectively. The radial transition densities for the target and projectile system have the form

$$g^{l_1s_0j,\,t_0}_{AB}(r_1)=\left\langle I_BT_B\left\|\sum_i\frac{\delta(r_1-r_i)}{r_i^2}T^{l_1s_0j}(i)\tau^{t_0}(i)\right\|T_AI_A\right\rangle , \quad (14)$$

$$g^{l_2s_0s,\,t_0}_{ab}(r_2)=\left\langle s_bt_b\left\|\sum_j\frac{\delta(r_2-r_j)}{r_j^2}T^{l_2s_0s}(j)\tau^{t_0}(j)\right\|t_as_a\right\rangle , \quad (15)$$

where T^{lsj} is the spherical tensor operator de-

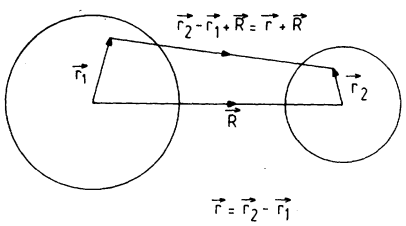

FIG. 1. Coordinates chosen in constructing the microscopic direct charge exchange form factors.

fined as[17]

$$T^{lsj}_{m_j} \equiv \sum_{m_l m_s} (lm_l sm_s | jm_j) i^l Y_{lm_l} \sigma^s_{m_s} . \quad (16)$$

The reduced matrix elements of Eq. (14) and (15) are reduced with respect to both total angular momentum and isospin, according to the definition of Brink and Satchler.[17] The l_1 and l_2 are the orbital angular momenta of the target and projectile, respectively. The d coefficients of Eq. (12) give us the selection rules for heavy-ion inelastic scattering as displayed in Fig. 2. These d coefficients become constant once a specific model is assumed to represent the internal motion of the involved nuclei. It is thus only desirable to mention in some detail the way to handle the folding integral of Eq. (13).

The folding integral of Eq. (13) can be easily evaluated by introducing the new coordinates $\vec{r} = \vec{r}_2 - \vec{r}_1$ (see Fig. 1), decomposing the solid harmonics $Y(\vec{r}_2) = r_2^l Y(\hat{r}_2)$ into $Y(\vec{r}_1)$ and $Y(\vec{r})$, and finally expanding v and $r_2^{-l_2} g_{ab}(r_2)$ in terms of spherical harmonics. The folding integral can then be given as

$$f^{jls,l_1l_2s_0t_0}(\vec{R}) = Y^*_{lm_l}(\hat{R}) \sum_{\lambda\lambda' k} a^{jls,l_1l_2s_0t_0}_{\lambda\lambda' k} \times I^{jls,l_1l_2s_0t_0}_{\lambda\lambda' k}(R) , \quad (17)$$

where

$$a^{jls,l_1l_2s_0t_0}_{\lambda\lambda' k} = \pi \delta_{\lambda+\lambda',l_2} \left[\frac{(2l_2+1)!}{(2\lambda+1)!(2\lambda'+1)!}\right]^{1/2} \hat{l}_1 \hat{l}_2 \hat{l}^{-1} \hat{\lambda}\hat{\lambda}' \hat{k} (l_1 0 \lambda 0 | k0)(k0\lambda' 0 | l0) W(l_1 \lambda l \lambda'; k l_2) \quad (18)$$

and

$$I^{jls,l_1l_2s_0t_0}_{\lambda\lambda' k} = \int dr\, r^{\lambda'+2} \bar{v}^l(R,r) \int dr_1 \bar{g}^k_{ab}(r,r_1) g_{AB}(r_1) r_1^{\lambda+2} , \quad (19)$$

where the Legendre coefficients $\bar{v}^l$ and $\bar{g}^k_{ab}$ are defined as

$$\bar{v}^l(R,r) \equiv \int_{-1}^{+1} v(|\vec{R}+\vec{r}|) P_l(\cos\theta) d(\cos\theta) , \quad (20)$$

$$\bar{g}^k_{ab}(r_1,r) \equiv \int_{-1}^{+1} g_{ab}(|\vec{r}+\vec{r}_1|)\, (|\vec{r}+\vec{r}_1|)^{-l_2} \times P_k(\cos\theta) d(\cos\theta) . \quad (21)$$

The vector coupling schemes appearing in d and a coefficients are collectively displayed in Fig. 2.

IV. NUMERICAL CALCULATIONS

A. One-step DWBA analysis

The microscopic one-step DWBA calculations have been performed for the reaction ^{28}Si(^{18}O,^{18}F)^{28}Al leading to the 3^+ ground and 2^+ excited doublet state, following the formulation outlined in the previous section. The (^{18}O,^{18}F) reaction gives the spin and isospin flip simultaneously and can thus be produced only by the $(\vec{\sigma}\cdot\vec{\sigma})(\vec{\tau}\cdot\vec{\tau})$ term in the nucleon-nucleon two-body force [Eq. (9)] in the simple one-step charge exchange model.

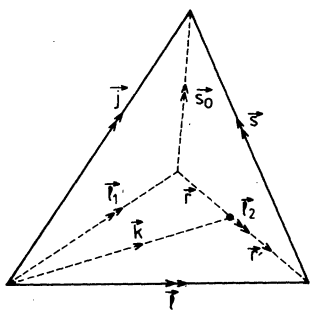

FIG. 2. Selection rules for the direct charge exchange process.

The radial form of interaction has been chosen as either Gaussian or Yukawa type:

$$v(r) = \exp\left(-\frac{r^2}{\beta^2}\right), \text{ with } \beta = 1.8 \text{ fm}$$

$$v(r) = \exp\left(-\frac{r}{\beta}\right) \Big/ \left(\frac{r}{\beta}\right) \text{ with } \beta = 1.0 \text{ fm} .$$

The strength parameter V_{11} in Eq. (9) is adjusted to fit the experimental data. Recently a new effective nucleon-nucleon interaction for inelastic scattering was introduced by Bertsch *et al.*[18] This interaction potential was derived by fitting the matrix elements of a sum of Yukawa potentials to various G-matrix elements. We also used this spin-isospin dependent central potential obtained from the even-state G-matrix elements of the Reid potentials as

$$v_{11}(r) = -2105.1 \frac{e^{-4r}}{4r} + 653.6 \frac{e^{-2.5r}}{2.5r} + 1.3 \frac{e^{-0.707r}}{0.707r} \text{ (MeV)} .$$

The ^{18}O and ^{18}F nuclei have been well understood by the shell model as comprising 2 nucleons in the s-d shell outside the ^{16}O core. They can be expressed in terms of the antisymmetric wave functions for the two nucleons in the s-d shell as

$$\Phi^{sm_st n_t} = \sum_{\mu_1\mu_2} C_{\mu_1\mu_2} | \mu_1\mu_2 sm_s tn_t \rangle ,$$

TABLE I. b coefficients for (^{18}O,^{18}F).

$l_2\, s_0\, s$	^{18}O \ ^{18}F	$(d_{5/2})^2$	$(s_{1/2})^2$	$(d_{3/2})^2$	$(d_{5/2}, d_{3/2})$	$(s_{1/2}, d_{3/2})$
0 1 1	$(d_{5/2})^2$	−0.3434			−0.2860	
	$(s_{1/2})^2$		−0.1605			
	$(d_{3/2})^2$			0.0050	0.1116	
2 1 1	$(d_{5/2})^2$	0.1388			−0.1011	
	$(s_{1/2})^2$					0.0320
	$(d_{3/2})^2$			−0.0071	0.0395	0.0200

where μ stands for the quantum numbers nlj, in the usual notation, which describe the single-particle wave motion, and $C_{\mu_1\mu_2}$ is the amplitude of each configuration. Then the radial transition density for the projectile system becomes

$$g_{ab}^{l_2 s_0 s, t_0}(r_2) = \sum_{\mu_1\mu_2} b_{\mu_1\mu_2}\phi_{\mu_1}(r_2)\phi_{\mu_2}(r_2)$$

$$b_{\mu_1\mu_2}^{ab} = \sqrt{2}\, C_{\mu_1\mu_2}^{b} C_{\mu_2\mu_2}^{a}(-)^{j_1+j_2} \times(1+\delta_{\mu_1\mu_2})^{1/2}\hat{j}_1\hat{j}_2^{-1}\langle j_1 \| T^{l_2 11} \| j_2\rangle ,$$

where ϕ_μ is the radial part of the single-particle wave function. The reduced spherical tensor matrix elements can be found in the tables of Bell and Satchler.[19] In this calculation, the shell-model wave functions of ^{18}O and ^{18}F were obtained from Kuo and Brown,[20] and the b coefficients are listed in Table I. ϕ_{μ_1} and ϕ_{μ_2} are generated from a Woods-Saxon potential, the geometry of which is $r_0 = r_c = 1.20$ fm and $a_0 = 0.65$ fm. The depth of the potential was determined from the experimental binding energies of the $1d_{5/2}$, $2s_{1/2}$, and $1d_{3/2}$ states in ^{17}O and ^{17}F, respectively. A spin orbit interaction of $V_{so} = 7$ MeV is used.

It was assumed that the ground state of ^{28}Si is a pure closed shell state and the $3^+,2^+$ ground state doublet of ^{28}Al consists of pure $(2s_{1/2})(1d_{5/2})^{-1}$ configurations. This assignment is basically consistent with shell model calculations[21] and earlier works[10,22] for charge exchange reactions. The b coefficients can be given as

$$b_{\mu_1\mu_2}^{AB} = 2\sqrt{3}\,\hat{I}_B^{-1}\langle 2s_{1/2} \| T^{1 1 j} \| 1d_{5/2}\rangle$$

and are tabulated in Table II. The radial single-particle form factors are generated in the same way as those in the projectile system.

In Table III, we summarize various angular momentum combinations and corresponding d and a coefficients [Eqs. (12) and (18)]. The radial form factors in Eq. (11) are obtained numerically and the partial form factors are shown in Fig. 3. As can be seen, the general envelope of the form factor is surface peaked, just like nuclear inelastic form factors. The shapes generated with different interaction potentials are not different from each other.

TABLE II. b coefficients for (^{28}Si,^{28}Al).

$l_1\, s_0\, j$	^{28}Si \ ^{28}Al	$(d_{5/2})^5(s_{1/2})$
2 1 3	$(d_{5/2})^6$	0.9772
2 1 2	$(d_{5/2})^6$	−0.6180

It is worth noting that the $l_2 = 0$ contribution dominates for both 3^+ ground and 2^+ excited state. This can be easily understood from the fact that the single-particle charge exchange components interfere constructively to give the large form factor as seen in Fig. 4. On the other hand, the $l_2 = 2$ form factor suffers a small magnitude because the single-particle transition contributions interfere strongly destructively as shown in Fig. 5. This interference effect, of course, depends on the sign and amplitude of each configuration. However, since the shell model wave functions of ^{18}O and ^{18}F have been well understood and provided a good description for numerous nuclear reactions, the interference effect shown seems to still hold. In fact, it has also been shown[9,10] that the $l_< = I_B - 1$ contribution solely accounts for the experimental results of the ^{18}O(^{6}Li,^{6}He)^{18}F reaction leading to the I_B^+ final state. This transferred angular momentum selectivity could be a characteristic of direct charge exchange mode. The ^{18}O(^{3}He,t)^{18}F reaction, in which multi-step processes are strongly suggested, gives[23] the $l_>$ pattern to the same states mentioned above.

According to Eq. (11), the 3^+ and 2^+ differential cross sections are in the ratio

$$\frac{\sigma_{3^+}}{\sigma_{2^+}} \approx \left| \frac{\langle s_{1/2} \| T^{213} \| d_{5/2}\rangle}{\langle s_{1/2} \| T^{212} \| d_{5/2}\rangle} \right|^2 = \frac{7}{2}$$

if the $l = 4$ contribution to the 3^+ state is small, which is the case for the present reaction. In other words, this ratio is proportional to the square of the ratio of the reduced matrix elements of the spherical tensor $T^{l_1 s_0 j}$ of the 3^+ and 2^+ states. It is important to point out that this depends neither on the choice of optical model para-

TABLE III. d and a coefficients.

Transitions	jsl	js_0l_1	ss_0l_2	$d\times 5\sqrt{21}$	$\lambda\lambda' k$	$a\times\sqrt{70}/\pi$
^{28}Si(0$^+$)	312	312	110	$\sqrt{35}$	002	$\sqrt{70}$
$-^{28}$Al(3$^+$)		312	112	−1	002	−10
					111	−14
					113	−6
					202	−10
	314	312	112	$\sqrt{15}$	022	10
					113	20
					204	10
^{28}Si(0$^+$)	212	212	110	$\sqrt{35}$	002	$\sqrt{70}$
$-^{28}$Al(2$^+$)		212	112	3.5	022	−10
					111	−14
					113	−6
					202	−10

meters (OMP) nor on the assumptions about the two-body force. It suggests that the higher spin state may be more strongly populated than the lower one through the direct charge exchange mode. It is just due to the strength of single-particle transitions and is independent of the angular momentum selectivity appearing in a quasi-elastic process, which leads usually to weaker cross sections for higher angular momentum transfer.

These form factors were integrated into the DWBA program SATURN-MARS-I[24] to calculate the differential cross sections. The OMP set S-7 (see Appendix) and H-1,[25] which fit elastic scattering in the incident and exit channel, respectively, are used for calculating incident and exit channel distorted waves. We did not consider any spin and isospin dependent optical potential since the importance of such a potential has never been reported in heavy-ion reactions. The strength parameter V_{11}, which is directly proportional to the square root of the cross section, is adjusted to obtain the measured cross sections. In Fig. 6, we display the theoretical fit (solid line) with a Gaussian interaction ($r_0 = 1.8$ fm) to the experimental 3$^+$, 2$^+$ doublet state. Except at the very forward angles, the general fit to the cross section is acceptable. As far as the shape of angular distribution is concerned, the dependence on the choice of two-body interaction potential and/or optical model potential turns out to be not significant. It has been shown[26,27] that one can improve the fit at forward angles by performing

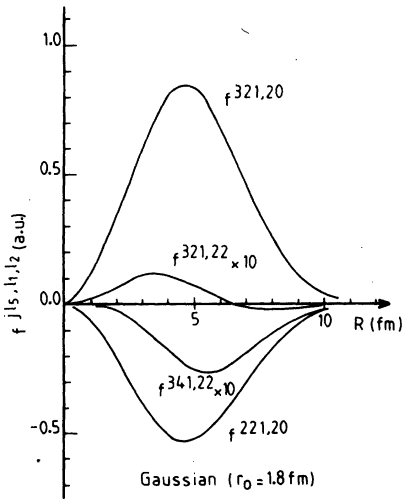

FIG. 3. Direct charge exchange radial form factors (in arbitrary units) for a different set of transferred angular momenta jls and the orbital angular momenta of target and projectile systems l_1 and l_2, respectively. The Gaussian interaction potential with a range parameter of 1.8 fm was used.

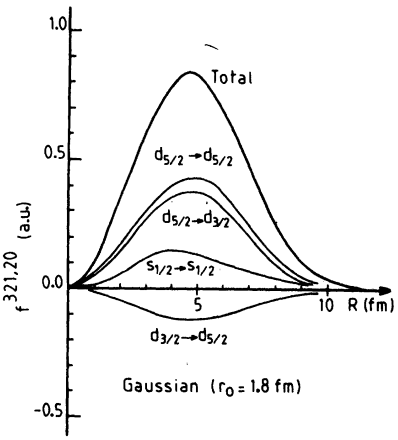

FIG. 4. $l_2 = 0$ radial form factors contributed from each single-particle transition in (^{18}O, ^{18}F) system. The single-particle transitions constructively interfere.

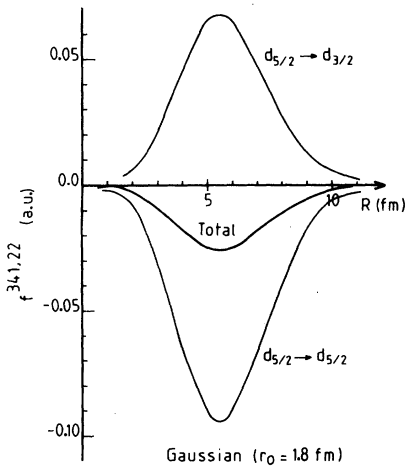

FIG. 5. $l_2=2$ radial form factors contributed from each single-particle transition in (^{18}O, ^{18}F) system. The single-particle transitions are small and destructively interfere.

coupled-channel Born approximation (CCBA) calculations taking into account the inelastic processes before and/or after the reaction takes place. We have not yet, however, performed CCBA calculations in order to improve the fit at forward angles. We present theoretical angular distributions of the 3$^+$ ground state (dashed line) and 2$^+$ excited state (dotted line) in Fig. 6. The shapes of the 3$^+$ and 2$^+$ state angular distributions are roughly the same and their ratio of magnitudes $\sigma_{3^+}/\sigma_{2^+}$ is about 3.5 as predicted earlier. One should remember that the $l=4$ contribution to the

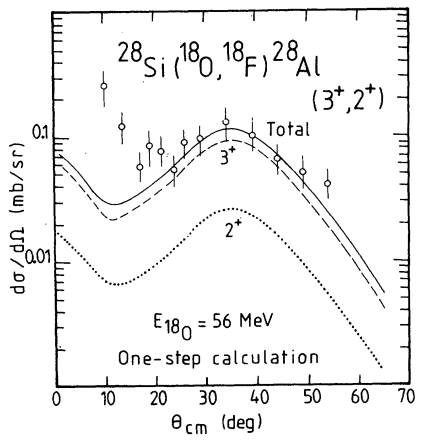

FIG. 6. The one-step DWBA fit (solid line) with the microscopic charge exchange form factors to the measured angular distribution of the 3$^+$, 2$^+$ ground state doublet. The dashed and dotted curves are the differential cross sections for the 3$^+$ and 2$^+$ state, respectively. The strength of spin-isospin dependent part of the two-body interaction potential V_{11} was adjusted to reach the measured cross section.

3$^+$ state is negligible.

The magnitude of the cross sections is one of the most important factors to test the reaction mechanism. The large uncertainty exists, unfortunately, in this direct charge exchange mode because of the lack of information about the nucleon-nucleon interaction potential and the nuclear wave functions of nuclei involved. However, in this particular choice of the reaction ^{28}Si(^{18}O,^{18}F)^{28}Al, the wave functions are relatively well known as mentioned earlier and only the pure V_{11} term contributes to the reaction. The only parameter we have adjusted is the strength of V_{11} to give the measured cross section. It is noted that the cross sections are proportional to V_{11}^2. We tabulate V_{11} obtained in this analysis in Table V, and compare it with the values from light-ion experiments. The present values are close to the larger limits from previous work.

The spin and isospin independent part V_{00} of the interaction potential by Bertsch *et al.* has been successful in explaining many elastic scattering data[28] with an improvement taking into account exchange effects.[29] Nevertheless the V_{11} part has not been tested experimentally except for very recent work of Williams-Norton *et al.*[10] on the reaction ^{40}Ca(^{7}Li,^{7}Be)^{40}K. The normalization factor N, which one is obliged to apply in order to reach the measured cross sections, is found to be 5.3 in this analysis. Williams-Norton *et al.* obtained N values ranging from 2 to 6 depending on the spin of the final state.

It has been reported that the strength of V_{11} for a given type of interaction and range parameter obtained from light-ion reactions varies as much as one order of magnitude depending strongly on the incident beam energy,[1] transferred angular momentum[9,10,30,31] and assumptions imposed on the nuclear wave functions,[9] and slightly on the size of target nucleus[9,10] and the choice of OMP sets.[29] The physics behind this variation has not yet been clarified.

Two additional calculations have been performed with a different OMP set and a different configuration for the nuclear wave functions, respectively. The OMP set E-18-3,[32] which also fits the entrance channel elastic scattering, was used for the entrance channel distorted waves. The V_{11} (Gaussian with a range parameter 1.8 fm) was larger by 22%. We made another calculation assuming pure ($d_{5/2}$) configurations in both ^{18}O and ^{18}F nuclei, but using OMP sets S-7 (entrance) and H-1 (exit). According to the shell model calculations in the s-d shell, this assumption is still good for the ^{18}O nucleus, but it can be assumed for ^{18}F only when the tensor force is not important.[20] The V_{11} (Gaussian with a range parameter 1.8 fm) ex-

TABLE IV. Optical model parameters.

System	V (MeV)	a_v (fm)	r_v [a] (fm)	W (MeV)	a_w (fm)	r_w (fm)	Set
^{28}Si + ^{18}O	−50.00	0.743	1.093	−43.02	0.743	1.093	S-7 [b]
	−19.13	0.547	1.384	−22.92	0.598	1.252	E-18-3 [c]
^{28}Al + ^{18}F	−100.00	0.550	1.220	−40.00	0.550	1.220	H-1 [d]

[a] $r_c = r_v$.
[b] Present experiment, see Appendix.
[c] M. C. Mermaz *et al.*, Phys. Rev. C 19, 794 (1979).
[d] W. R. McMurray *et al.*, Nucl. Phys. A265, 517 (1976).

tracted was decreased only by 7%. The angular shapes from both calculations were very similar to that in Fig. 6. It is thus concluded that the choice of OMP sets and the configuration mixing in the nuclear wave functions do not play a significant role in determining the strength of spin and isospin dependent central potential in this particular heavy-ion reaction. In the next subsection, we present a two-step analysis for this reaction.

B. Two-step EFR-DWBA analysis

The two-step EFR-DWBA calculations were also performed to describe this reaction by the stripping-pickup and pickup-stripping sequential mechanism mentioned in the previous section. The intermediate states considered are the following: (1) the (^{18}O,^{17}O) neutron stripping going to ^{29}Si followed by the (^{17}O,^{18}F) proton pickup leading to ^{28}Al, and (2) the (^{18}O,^{19}F) proton pickup going to ^{27}Al followed by the (^{19}F,^{18}F) neutron stripping leading to ^{28}Al. There are in fact many open channels leading to the states in ^{17}O and ^{19}F from ^{18}O ground states. However, we have only considered good single-particle states with a large spectroscopic factor. All the routes considered are summarized in Fig. 7.

The second order EFR-DWBA calculations have been made by taking up to the second iteration in a CRC code by Tamura, Udagawa, and Low.[33] The program has been modified such that several intermediate channels can be included simultaneously in the calculation, and the reaction leading to the nonzero spin state in the final residual nucleus can be studied. The bound state wave functions in calculating the EFR form factor $F^{jls}_{l_b,l_c}$ are generated in exactly the same way as those in the previous one-step DWBA calculations. The transferred angular momenta for each route and the spectroscopic factors used in the actual calculations are tabulated in Table VI. As will be shown in Appendix, we also studied ^{28}Si(^{18}O,^{17}O)^{29}Si and ^{28}Si(^{18}O,^{18}F)^{27}Al reactions and extracted the spectroscopic factors. These values are used in the actual calculations. The spectroscopic factors for the (^{17}O,^{18}F) system were obtained from Kuo and Brown.[20] Since the spectroscopic factors for the (^{19}F,^{18}F), (^{29}Si,^{28}Al), and (^{27}Al,^{28}Al) systems have not been well determined, they were simply chosen by assuming the same single-particle configuration as those of the (^{18}O,^{17}O), (^{28}Si,^{27}Al), and (^{28}Si,^{29}Si) systems, respectively. The OMP set S-7, which reproduces the elastic scattering data in the entrance channel, is constantly employed throughout all calculations. It is worth noting that there is no free parameter in these second-order DWBA calculations.

The transition amplitude of the second-order DWBA for each route is first calculated and the differential cross sections at $\theta_{c.m.} = 35°$ obtained from each transition amplitude are compared in

TABLE V. Strength parameter V_{11} in MeV of interaction potential. The OMP sets S-7 (entrance channel) and H-1 (exit channel) are used.

Interaction	(n,p) (Ref. 1)	(^{3}He,t) (Ref. 30)	(^{6}Li,^{6}He) (Ref. 9)	(^{7}Li,^{7}Be) (Ref. 10)	(^{18}O,^{18}F) (present)
Gaussian (r_0 = 1.8 fm)	7 ~ 21	16–45 [a]		6	25
Yukawa (r_0 = 1.0 fm)		10–30	25–250	15	76
Yukawas (Ref. 18) [b]				2–6 [c]	5.3

[a] Rescaled from r_0 = 1.7 fm to 1.8 fm.
[b] The theoretical values are multiplied by the normalization factor listed.
[c] The single-nucleon exchange effects were added to the interaction of Bertsch *et al.* (Ref. 18).

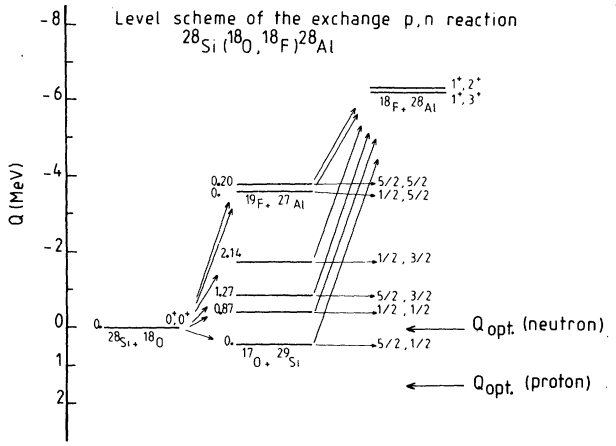

FIG. 7. Diagram of all channels included in the two-step calculations. The Q values involved are also inset.

Table VI. The contributions from the $^{17}O+^{29}Si$ intermediate channels yield small cross sections mainly due to the unfavorable Q values of the second step $^{29}Si(^{17}O,^{18}F)^{28}Al$ as can be seen in Fig. 7. Each intermediate channel contribution exhibits roughly the same shape of angular distributions. As far as the magnitude of the cross-section is concerned, angular momentum couplings and Q values for each intermediate channel make it complicated, and it can not be interpreted in terms of a single physical term such as the Q value or transferred angular momentum. The ratios between σ_{3^+} and σ_{2^+} for different intermediate channels also show irregularities.

The transition amplitudes from all 6 intermediate channels considered are coherently added, according to Eq. (4), to obtain the final cross sections. Those from different routes near the grazing waves turn out to be almost parallel to each other and thus constructively interfere. It leads to large final cross sections, for instance $\sigma_{3^+}(\theta_{c.m.}=35°)=13.46$ μb, and $\sigma_{2^+}(\theta_{c.m.}=35°)=5.58$ μb. The sum of the individual cross sections of the 3^+ and 2^+ states is normalized to reach the experimental cross sections. The normalization factor N ($\sigma_{exp}=N\sigma_{theo}$) is found to be 5.8. Such a theoretical fit (solid line) is displayed in Fig. 8 along with the theoretical 3^+ (dashed line) and 2^+ (dotted line) angular distributions. The shape of the angular distributions is almost the same as that obtained from one-step calculations, but has a little broader bell shape. It is probably due to the dispersive effect[34,35] which is associated with the fact that the interaction region is often narrower for a two-step than for a one-step process. The cross section ratio between the 3^+ and 2^+ states turns out to be 2.4, compared to 3.5 from one-step calculations.

V. DISCUSSION AND CONCLUSION

Our measured angular distribution shows a bell shape peaked at the grazing angle in the exit channel as has been shown in many heavy-ion induced transfer reactions. It does not exhibit a specific transferred orbital angular momentum character. The absolute magnitude of the cross sections is thus the only factor which can test which reaction process dominates.

Both one-step direct and two-step successive ap-

TABLE VI. Transferred orbital angular momenta for each route and the spectroscopic factors used in the actual calculations. The subscripts S, 1, and 2 denote the projectile-ejectile and target-residual system, respectively. The i and f stand for the initial (first) step and final (second) step, respectively. The differential cross sections at $\theta_{c.m.}=35°$ were obtained from a calculation considering only one intermediate channel.

Intermediate channel	Spectroscopic factors				g.s. 3^+		0.03 MeV 2^+	
	S_{1i}	S_{2i}	S_{1f}	S_{2f}	$l_i\,l_f\,l$	σ (μb)	$l_i\,l_f\,l$	σ (μb)
$^{17}O(\frac{5^+}{2})+^{29}Si(\frac{1^+}{2})$	1.77	0.56	0.53[a]	3.80[b]	244	0.06	242	0.06
$^{17}O(\frac{1^+}{2})+^{29}Si(\frac{1^+}{2})$	0.23	0.56	0.26[a]	3.80[b]	022	0.40	022	0.16
$^{17}O(\frac{5^+}{2})+^{29}Si(\frac{3^+}{2})$	1.77	0.73	0.53[a]	3.80[b]	444	0.25	442	0.07
$^{17}O(\frac{1^+}{2})+^{29}Si(\frac{3^+}{2})$	0.23	0.73	0.26[a]	3.80[b]	224	0.15	222	0.40
$^{19}F(\frac{1^+}{2})+^{27}Al(\frac{5^+}{2})$	0.33	3.80	0.23[c]	0.56[d]	202	0.65	202	0.19
$^{19}F(\frac{5^+}{2})+^{27}Al(\frac{5^+}{2})$	0.39	3.80	1.77[c]	0.56[d]	424	1.71	422	0.30

[a] T. T. S. Kuo and G. E. Brown, Nucl. Phys. 85, 40 (1966).
[b] Assumed from the proton configuration of the (^{28}Si-^{27}Al) system.
[c] Assumed from the neutron configuration of the (^{18}O-^{17}O) system.
[d] Assumed from the neutron configuration of the (^{28}Si-^{29}Si) system.

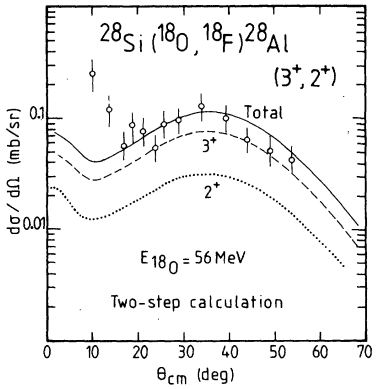

FIG. 8. The two-step second order DWBA fit (solid line) with the EFR form factor to the measured angular distributions of the 3^+, 2^+ ground state doublet. The dashed and dotted curves are the differential cross sections for the 3^+ and 2^+ state, respectively. The theoretical curves are normalized to the experimental cross sections with $N = \sigma_{exp}/\sigma_{theo} = 5.8$.

proaches reproduce the general shape of the measured angular distribution with the same quality. The strength of the spin-isospin dependent term was deduced on the basis of microscopic one-step direct charge exchange mode, and compared with that extracted from various experiments. The value reported has a wide range of uncertainties, of which the origin is not well understood at present. Little theoretical work has been accumulated either. Our value is within this range but close to the upper limit of uncertainty. Our two-step calculation, considering both successive one-nucleon pickup and stripping, and stripping and pickup reactions, shows its significance in explaining the magnitude of the measured cross sections, even though it cannot safely be judged the dominant reaction process.

The ratio between the 3^+ and 2^+ cross section is expected to be 3.5 according to the direct charge exchange model. This ratio is not related to the

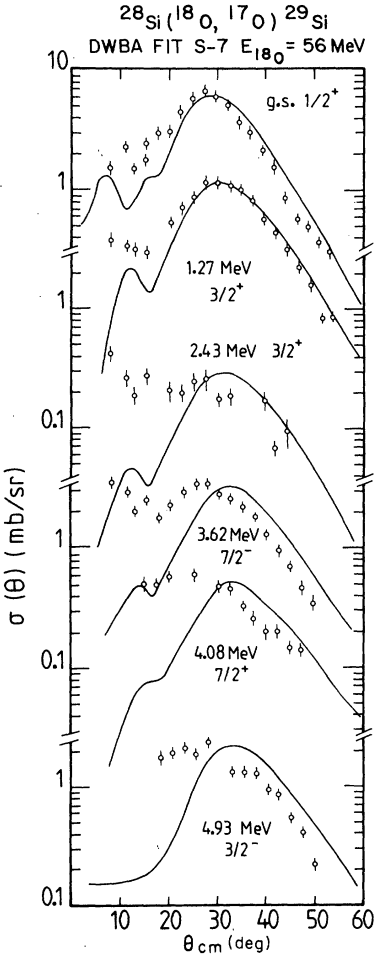

FIG. 9. EFR-DWBA fits to the experimental angular distributions of $^{28}Si(^{18}O, ^{17}O)^{29}Si$ one neutron stripping reaction.

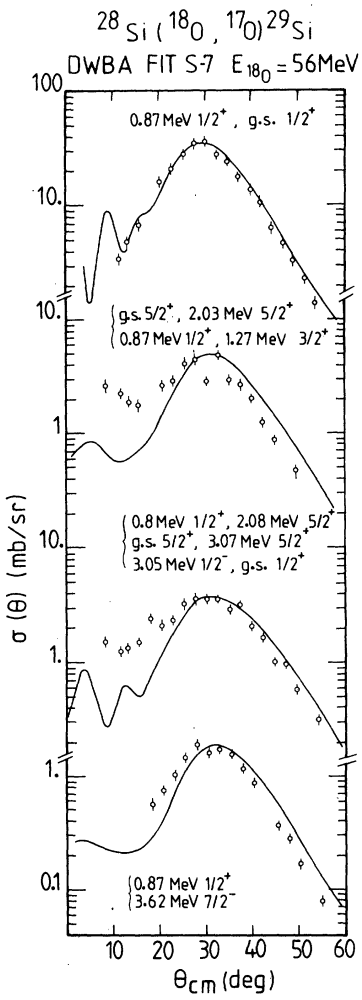

FIG. 10. Same as Fig. 9.

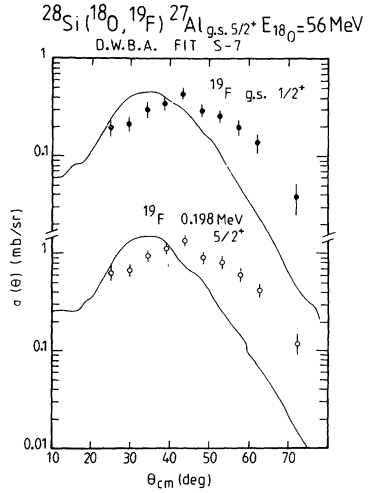

FIG. 11. EFR-DWBA fits to the experimental angular distributions of the ^{28}Si(^{18}O, ^{19}F)^{27}Al one proton pickup reaction.

particular choice of interaction potential, but solely originated from the nuclear structure. Our two-step calculation gives a ratio of 2.4. We might thus say experimentally which process is favorable by comparing accurately measured cross sections for these two states. Unfortunately, however, the present experiment could not resolve these two states separated 31 keV from each other.

As a remedy for the uncertainty of V_{11}, it has been suggested[2,31] that the tensor force in the nucleon-nucleon two-body interaction may play a significant role in accounting for the nuclear charge exchange reaction, especially leading to unnatural parity states. As discussed earlier, we had a calculation assuming a pure $(d_{5/2})^2$ configuration for the ground state of ^{18}F neglecting the tensor force effect. The result shown was not much different from the previous calculation. Since the tensor term was not explicitly introduced in our calculations, the role of tensor force would still not be ruled out. A study on the role of tensor force in heavy-ion charge exchange reaction is in progress.

It has become obvious recently that the DWBA theory works well only when the l- and Q-matching conditions are fulfilled.[35,36] This is probably one of the reasons why the reported V_{11} value has an unphysical dependence on the transferred angular momentum. The reaction ^{28}Si(^{18}O,^{18}F)^{28}Al is actually a badly l- and Q-matched reaction, mismatched by about $4\hbar$ and 6 MeV respectively. This fact reduces the credibility of V_{11} extracted from our direct charge exchange analysis.

It is our conclusion that multi-step successive nucleon transfer processes should be emphasized in explaining the heavy-ion charge exchange reactions. The use of heavy-ion as a projectile for the study of nuclear charge exchange reactions provides a chance uniquely to determine the V_{11} term in the nucleon-nucleon two-body interaction, but the two-step contributions and the role of tensor force should be taken into account in the analysis in order to extract a dependable spin-isospin dependent two-body interaction.

TABLE VII. Spectroscopic factors deduced from this analysis.

Transitions	Light-ion exp.	Present
^{28}Si(g.s. 0$^+$)–^{29}Si(g.s. $\frac{1}{2}^+$)	0.53 [a]	0.56
–^{29}Si(1.27 MeV $\frac{3}{2}^+$)	0.73 [a]	0.73
–^{29}Si(3.62 MeV $\frac{7}{2}^+$)	0.38 [a]	0.51
–^{29}Si(4.08 MeV $\frac{7}{2}^+$)	···	0.06
–^{29}Si(4.93 MeV $\frac{3}{2}^-$)	0.56 [a]	0.40
^{18}O(0$^+$ g.s.)–^{17}O(g.s. $\frac{5}{2}^+$)	1.31 [b]	1.77
–^{17}O(0.87 MeV $\frac{1}{2}^+$)	0.07 [b]	0.23
^{28}Si(0$^+$ g.s.)–^{27}Al(g.s. $\frac{5}{2}^+$)	3.8 [c]	3.8
^{18}O(0$^+$ g.s.)–^{19}F(g.s. $\frac{1}{2}^+$)	0.21 [d]	0.33
–^{19}F(0.20 MeV $\frac{5}{2}^+$)	0.41 [d]	0.39

[a] M. C. Mermaz *et al.*, Phys. Rev. C 4, 1778 (1971).
[b] M. Pignanell *et al.*, Phys. Rev. C 8, 2120 (1973).
[c] B. H. Wildenthal and E. Newman, Phys. Rev. 167, 1027 (1968).
[d] F. Ajzenberg-Selove, Nucl. Phys. A300, 106 (1978).

We are very grateful to Dr. E. Müller for helpful discussions and a careful reading of this manuscript.

APPENDIX

The $^{28}Si(^{18}O,^{17}O)^{29}Si$ and $^{28}Si(^{18}O,^{19}F)^{27}Al$ reactions have been measured at 56 MeV incident beam energy. Most of the single particle and hole states, respectively, are strongly populated as seen in the light-ion as well as heavy-ion reactions. We have further measured simultaneously the transfer reaction leading to the ground state and the first excited state in ^{17}O. All these data are analyzed on the basis of EFR-DWBA formalism using the computer code SATURN-MARS-I.[24] The OMP set S-7, which accounts well for the elastic scattering of the entrance channel, has been used in generating distorted waves in both entrance and exit channel. The results of those analyses are presented in Figs. 9, 10, and 11. The extracted spectroscopic factors for the ^{28}Si-^{29}Si, ^{28}Si-^{27}Al, ^{18}O-^{17}O, and ^{18}O-^{19}F systems are tabulated in Table VII. Agreements with those from light-ion experiments are good. These spectroscopic factors have been integrated into our analysis of the charge exchange reaction $^{28}Si(^{18}O,^{18}F)^{28}Al$.

---

*Present address: Universidade de São Paulo, Institut de Fisica, Cidade Universitaria, 05508 São Paulo, Brazil.

†Permanent address: Jabatan Fizik, University Malaya, Kuala Lumpur, Malaysia.

[1]T. Une, S. Yamaji, and H. Yoshida, Prog. Theor. Phys. 35, 1010 (1966).

[2]E. Rost and P. D. Kunz, Phys. Lett. 30B, 231 (1969).

[3]E. R. Flynn, J. Sherman, and N. Stein, Phys. Rev. Lett. 32, 846 (1974).

[4]K. Bharuth-Ram, S. M. Perez, F. D. Brooks, S. A. R. Wynchank, and W. R. McMurray, Nucl. Phys. A278, 285 (1977).

[5]R. Schaeffer and N. K. Glendenning, Nucl. Phys. A207, 321 (1973).

[6]M. Toyama, Phys. Lett. 38B, 147 (1972).

[7]W. R. Coker, T. Udagawa, and H. H. Wolter, Phys. Rev. C 7, 1154 (1973).

[8]H. H. Duhm, H. Hafner, R. Renfordt, M. Goldschmidt, O. Dragun, and K.-I. Kubo, Phys. Lett. 48B, 1 (1974).

[9]W. R. Wharton and P. T. Debevec, Phys. Rev. C 11, 1963 (1975).

[10]M. E. Williams-Norton, F. Petrovich, K. W. Kemper, G. M. Hudson, R. J. Puigh, and A. F. Zeller, Nucl. Phys. A275, 509 (1977); A313, 477 (1979).

[11]J. B. Marion and F. C. Young, *Nuclear Reaction Analysis* (North-Holland, Amsterdam, 1968).

[12]D. J. Weber, N. M. Hintz, and D. Dehnhard, Nucl. Instrum. Methods 124, 317 (1975).

[13]U. Gotz, M. Ichimura, R. A. Broglia, and A. Winther, Phys. Rep. C16, 115 (1975).

[14]D. H. Feng, T. Udagawa, and T. Tamura, Nucl. Phys. A274, 262 (1976).

[15]T. Tamura, Phys. Rep. C14, 59 (1974).

[16]F. Petrovich and D. Stanley, Nucl. Phys. A275, 487 (1977).

[17]D. M. Brink and G. R. Satchler, *Angular Momentum*, 2nd edition (Oxford University Press, Oxford, 1971).

[18]G. Bertsch, J. Borysowich, H. McManus, and W. G. Love, Nucl. Phys. A284, 399 (1977).

[19]W. K. Bell and G. R. Satchler, Nucl. Data Tables A9, 147 (1971).

[20]T. T. S. Kuo and G. E. Brown, Nucl. Phys. 85, 40 (1966).

[21]B. H. Wildenthal and J. B. McGrory, Phys. Rev. C 7, 714 (1973).

[22]A. Agodi, R. Giordano, and G. Schiffrer, Nucl. Phys. 46, 545 (1963).

[23]H. H. Duhm, K. Peterseim, R. Seehars, R. Finlay, and C. Detraz, Nucl. Phys. A151, 579 (1970).

[24]T. Tamura and K. S. Low, Comput. Phys. Commun. 8, 349 (1974).

[25]W. R. McMurray, T. W. Conlon, B. W. Hooton, and M. Ivanovich, Nucl. Phys. A265, 517 (1976).

[26]T. Udagawa and T. Tamura, Phys. Lett. 57B, 23 (1975).

[27]J. C. Peng, B. T. Kim, M. C. Mermaz, A. Greiner, and N. Lisbona, Phys. Rev. C 18, 2179 (1978).

[28]W. G. Love, in *Proceedings of the Symposium on Heavy-Ion Elastic Scattering* (Rochester, New York, 1977) and references therein.

[29]G. R. Satchler and W. G. Love, Phys. Lett. 65B, 415 (1976).

[30]P. Kossanyi-Demay, P. Roussel, H. Faraggi, and R. Schaeffer, Nucl. Phys. A148, 181 (1970).

[31]G. Bruge, M. S. Zisman, A. D. Bacher, R. Schaeffer, C. J. Zeippen, and J. M. Loiseaux, Phys. Rev. C 19, 9 (1979).

[32]M. C. Mermaz, M. A. G. Fernandes, A. Greiner, B. T. Kim, and N. Lisbona, Phys. Rev. C 19, 794 (1979).

[33]T. Tamura, T. Udagawa, and K. S. Low, private communication.

[34]H. L. Harney, P. Braun-Munzinger, and C. K. Gelbke, Z. Phys. 269, 339 (1974).

[35]T. Udagawa, in *Proceedings of the International Conference on Nuclear Structure, Tokyo, 1977*, edited by T. Marumori (Physical Society of Japan, Tokyo, 1978), p. 667.

[36]D. G. Kovar, W. Henning, B. Zeidman, Y. Eisen, J. R. Erskine, H. T. Fortune, T. R. Ophel, P. Sperr, and S. E. Vigdor, Phys. Rev. C 17, 83 (1978).